Determination of the nucleon-nucleon interaction in the ImQMD model by nuclear reactions at the Fermi energy region [*]

LI Cheng(李成)[1,2;1]   TIAN Jun-Long(田俊龙)[2;2]   QIN Yu-Jiao(秦玉娇)[1]
LI Jing-Jing(李静静)[2]   WANG Ning(王宁)[1;3]

[1] Department of Physics, Guangxi Normal University, Guilin 541004, China
[2] School of Physics and Electrical Engineering, Anyang Normal University, Anyang 455000, China

Abstract: The nucleon-nucleon interaction is investigated by using the improved quantum molecular dynamic (ImQMD) model with three sets of parameters IQ1, IQ2 and IQ3, in which the corresponding incompressibility coefficients of nuclear matter are different. The charge distributions of fragments are calculated for various reaction systems at different incident energies. The parameters strongly affect the charge distributions and the fragment multiplicity spectrum below the threshold energy of nuclear multifragmentation. The fragment multiplicity spectrum for ^{238}U+^{197}Au at 15 A MeV and the charge distributions for ^{129}Xe+^{120}Sn at 32 and 45 A MeV, and ^{197}Au+^{197}Au at 35 A MeV are reproduced by the ImQMD model with the set of parameter IQ3. It is found that: 1) The charge distribution of the fragments and the fragment multiplicity spectrum are good observables for testing the model and the parameters. 2) The Fermi energy region is a sensitive energy region for studying nucleon-nucleon interaction.

Key words: nucleon-nucleon interaction, heavy-ion collision, ImQMD model

PACS: 25.70.-z, 25.70.Mn, 25.70.Pq   **DOI:** 10.1088/1674-1137/37/11/114101

1   Introduction

The nucleon-nucleon (N-N) interaction is the most fundamental problem in nuclear physics. It is related to many nuclear properties and nuclear reaction mechanisms, for example, the binding energies [1–3], incompressibility coefficient [4–9], nuclear structure [10–12], fusion-fission reactions [13–15] and so on. Therefore, the knowledge of the N-N interaction is of great significance for the community to explain the nature of the nucleus and study nuclear reaction mechanism. The Skyrme force is an effective parameterization N-N interaction that has been proposed based on the G-matrix for nuclear Hartree-Fock calculations reproducing the basic nuclear structure (masses, radii and other physical quantities). Since Vautherin and Brink [16] performed fully microscopic self-consistent mean-field Hartree-Fock calculations with the Skyrme type effective nucleon-nucleon interaction [17–19], many different parameters of the Skyrme interaction have been proposed, such as SkP, SkM*, Sly1-7 [7–9]. The improved quantum molecular

dynamic (ImQMD) model adopts the Skyrme type effective interaction and is successfully used in intermediate-energy heavy-ion collisions and fusion reactions at energies near the Coulomb barrier [20–23]. By combining the known Skyrme forces and the experimental data for fusion reactions and heavy-ion collisions at intermediate energies, three sets of different parameters, IQ1, IQ2 and IQ3, are proposed [21, 24, 25]. The different ImQMD parameters correspond to the different N-N interactions and different nuclear equations of state (EOS).

In low energy heavy-ion collision, the reaction system has a low excitation energy, and one observes the emission of light particles plus an evaporation residue for light systems or fission caused by Coulomb repulsion for heavy systems. As the incident energy increases to a threshold energy, the excitation energy of the reaction system will reach the maximum limit. It implies that the nuclear reaction will enter the multifragmentation process. In order to investigate N-N interaction, we will study the charge distributions of fragments for various reaction systems at different incident energies and the

fragment multiplicity spectrum for ^{238}U+^{197}Au at 15 A MeV with the ImQMD model by adopting different parameters. The structure of this paper is as follows: In Section 2, relation of EOS and wave-packet width is briefly introduced. In Section 3, three sets of ImQMD parameters IQ1, IQ2 and IQ3 will be employed to calculate charge distribution for ^{40}Ca+^{40}Ca with incident energy from 10 to 45 A MeV, ^{129}Xe+^{120}Sn at 32 and 45 A MeV, ^{197}Au+^{197}Au at 35 and 50 A MeV, and fragment multiplicity spectrum at 15 A MeV for ^{238}U+^{197}Au. Finally, a summary is given in Section 4.

2   EOS and wave-packet width

The EOS of nuclear matter plays an important role in the study of nuclear properties, heavy-ion collisions, neutron stars and supernovae. The EOS depends on the interactions of the particles in the matter, which describes how the state of the matter changes under different conditions. For cold nuclear matter, the EOS is usually defined as the binding energy per nucleon as a function $E/A = \varepsilon(\rho, T, \delta)$ of the density ρ, temperature T and isospin asymmetry $\delta = (\rho_n - \rho_p)/\rho$. For the symmetric nuclear matter $\delta = 0$ [6], there are empirical values of the nuclear matter EOS such as energy per nucleon $\varepsilon_0 \approx -16$ MeV, incompressibility $K_\infty \approx 230$ MeV and saturation density of symmetric nuclear matter $\rho_0 \approx 0.16$ fm^{-3} at $T = 0$ MeV. However, the uncertainty of EOS still causes some difficulties for an unambiguous determination of the model parameters. In the ImQMD model, the equation of state of the symmetric nuclear matter can be expressed as [24, 26]

$$\frac{E(\rho)}{A} = \xi c_k \rho^{2/3} + \frac{1}{2}\alpha\frac{\rho}{\rho_0} + \beta\frac{\rho^\gamma}{(\gamma+1)\rho_0^\gamma} + g_\tau\frac{\rho^\eta}{\rho_0^\eta}, \quad (1)$$

where $\xi = c_0/c_k$,

$$c_k = \frac{3}{5}\frac{\hbar^2}{2m}\left(\frac{3\pi^2}{2}\right)^{2/3} = 75.0 \text{ MeV·fm}^{-2}.$$

The coefficient c_0 can be determined by the kinetic energies of nuclei at their ground state [26]. The density distribution function ρ of a system can be read

$$\rho(\boldsymbol{r}) = \sum_i \frac{1}{(2\pi\sigma_r)^{3/2}}\exp\left[-\frac{(\boldsymbol{r}-\boldsymbol{r}_i)^2}{2\sigma_r^2}\right]. \quad (2)$$

Figure 1 shows the energy per nucleon of symmetric nuclear matter as a function of ρ/ρ_0. It is seen that the EOS with the IQ3 is clearly harder than that with the IQ1 and IQ2 in region $\rho/\rho_0 > 1$ with the increase

of the density, which is due to the larger incompressibility coefficient of 226 MeV for IQ3 compared to IQ2 (195 MeV) and IQ1 (165 MeV). In the heavy-ion collision process, the projectile and target first contacted, then compressed and then expanded. The soft nuclear matter have a higher compression density and more violent expansion process. While for the finite nuclear system, the expansion process will be influenced by the nuclear surface energy, Coulomb energy and wave-packet width, etc.

In the ImQMD model, each nucleon is described by a coherent state of Gaussian wave packet. The system-size-dependent wave-packet width in coordinate space is given by the formula [27]:

$$\sigma_r^n = \sigma_0 + \sigma_1 A_n^{1/3}, \quad n = \{p, t\}. \quad (3)$$

Here, σ_r^p (σ_r^t) denotes the wave-packet width for the nucleons which belong to the projectile (target). A_p and A_t denote the mass number of the projectile and target, respectively. For symmetric reaction systems, $\sigma_r = \sigma_r^p = \sigma_r^t$. The parameters σ_0 and σ_1 have been listed in Table 1. The wave-packet width is useful for exploring the influence of the interaction range of nucleons and the finite-size effect of nuclei. In Fig. 2, we show the wave-packet width of nucleon as a function of system-size with the three sets of parameters. One can see from the figure that there is a large difference with the different system. The wave-packet width given by the IQ1 and IQ2 obviously is higher than the IQ3 with increasing mass number. The three sets of parameters are also listed in Table 1.
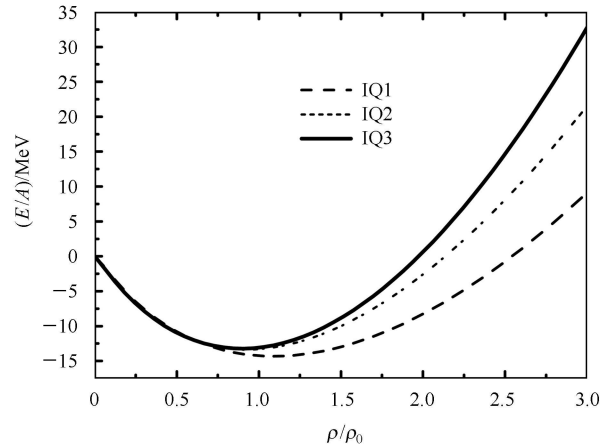

Fig. 1.   Energy per nucleon of symmetric nuclear matter for different parameters.

Table 1.   The ImQMD parameters.

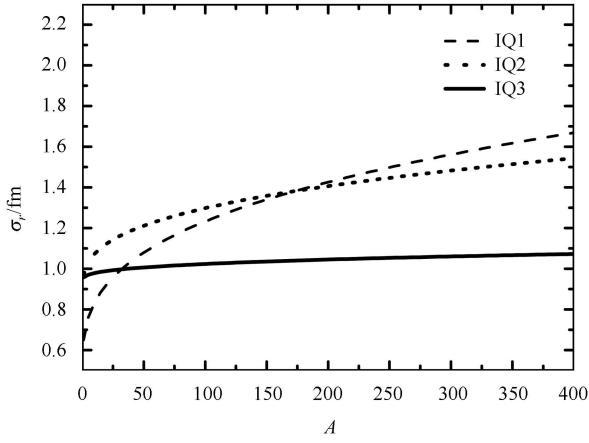|	α/MeV	β/MeV	γ	g_0/(MeV·fm^2)	g_τ/MeV	η	C_S/MeV	κ_s/fm^2	ρ_0/fm^{-3}	σ_0/fm	σ_1/fm
IQ1	-310	258	7/6	19.8	9.5	2/3	32.0	0.08	0.165	0.49	0.16
IQ2	-356	303	7/6	7.0	12.5	2/3	32.0	0.08	0.165	0.88	0.09
IQ3	-207	138	7/6	18.0	14.0	5/3	32.0	0.08	0.165	0.94	0.018

Fig. 2.   Wave-packet width as a function of system-size with the three sets of parameters.

3   Results

Based on the ImQMD model, the charge distribution of fragments for different reaction systems will be employed to explore the N-N interaction. We present the charge distribution of fragments for ^{40}Ca+^{40}Ca at incident energy of 35 A MeV in Fig. 3. The solid triangles, solid squares and solid stars denote the simulation results with the IQ1, IQ2 and IQ3, respectively. The open circles denote the experimental data [28]. Here we create 500 events for central collisions and for each event we simulate the whole collision process until $t=3000$ fm/c without combining statistical models. From Fig. 3(a–c), one sees that the experimental data can be reproduced very well with the ImQMD calculations with three sets of parameters. However, their EOS and the wave-packet width are different. Why do they have a similar charge distribution?
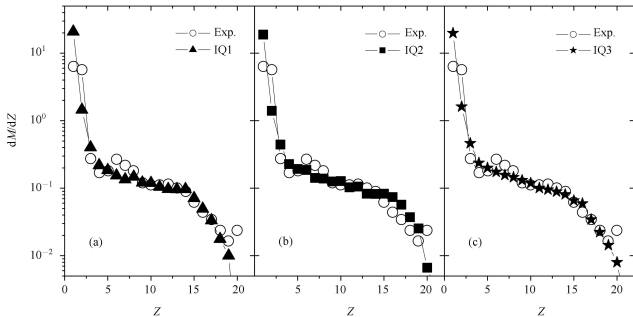

Fig. 3.   Charge distribution of fragments from three sets of parameters for ^{40}Ca+^{40}Ca at incident energy of 35 A MeV.

For further investigating the effect of N-N interaction on the heavy-ion collisions, we studied the charge distribution of fragments for different reaction systems at different incident energies. In Fig. 4 we show the charge distribution of fragments calculated by the ImQMD model

with three sets of parameters for ^{40}Ca+^{40}Ca at incident energies from 10 to 45 A MeV. One sees that the charge distribution of fragments are closed to each other at the energy region 35–45 A MeV, but there exist significant differences at the energy region 10–30 A MeV for three sets of parameters, IQ1, IQ2 and IQ3. The peaks for the IQ1, IQ2 and IQ3 are all becoming gradually lower with increasing incident energies from 10 A MeV to 30 A MeV. It implies that 10–30 A MeV is the transition region of the fusion reaction to the multifragmentation for ^{40}Ca+^{40}Ca reaction system. The fusion evaporation of the reaction system is strongly affected by the ImQMD parameters. Above 30 A MeV, the nuclear reaction turns to the multifragmentation, the distribution of fragments is not sensitive to the ImQMD parameters.

Figure 5 shows the charge distribution of fragments for ^{129}Xe+^{120}Sn at 32 and 45 A MeV [29], ^{197}Au+^{197}Au at 35 [30, 31] and 50 A MeV, which are calculated by the ImQMD model using three sets of parameters. One can see that the charge distribution of fragments at 45 A MeV for ^{129}Xe+^{120}Sn and 50 A MeV for ^{197}Au+^{197}Au are also relatively close to each other calculated by three sets of parameters, while there are still significant differences at the lower incident energy of 32 A MeV for ^{129}Xe+^{120}Sn reaction and 35 A MeV for ^{197}Au+^{197}Au reaction. Comparing ^{129}Xe+^{120}Sn and ^{197}Au+^{197}Au reaction system with ^{40}Ca+^{40}Ca, we find that the sensitive energy region for the ImQMD parameters depends on the reaction systems. This is due to the Coulomb repulsion of heavier systems being observably larger than that of the lighter system, such as, the Bass barrier is 661.8 MeV for ^{197}Au+^{197}Au and 53.5 MeV for ^{40}Ca+^{40}Ca. By comparing with the experimental results, we find that the experimental data can be reproduced well with IQ3. It seems that IQ3 is a set of suitable parameters in the ImQMD model for heavy-ion collisions.

In order to further test the above conclusion, we study the fragment multiplicity spectrum of ^{238}U+^{197}Au reaction by using three sets of parameters. In Fig. 6, we show the comparison of calculated results with the experimental data for fragment multiplicity spectrum of ^{238}U+^{197}Au reaction at 15 A MeV. The open squares, open triangles, solid stars and open circles denote the results with IQ1, IQ2, IQ3 and the experimental data [32], respectively. We created 4000 events from central to peripheral collisions and counted the number of fragments in each reaction except in the case where the charge $Z<8$ as that did in the experiment. The experimental data shows that two-body events exhaust only about 5% and the three- and four-body events exhaust approximately 83% of the total reaction events. From Fig. 6, one can see that the experimental data can be reasonably well reproduced by using the ImQMD model with IQ3.
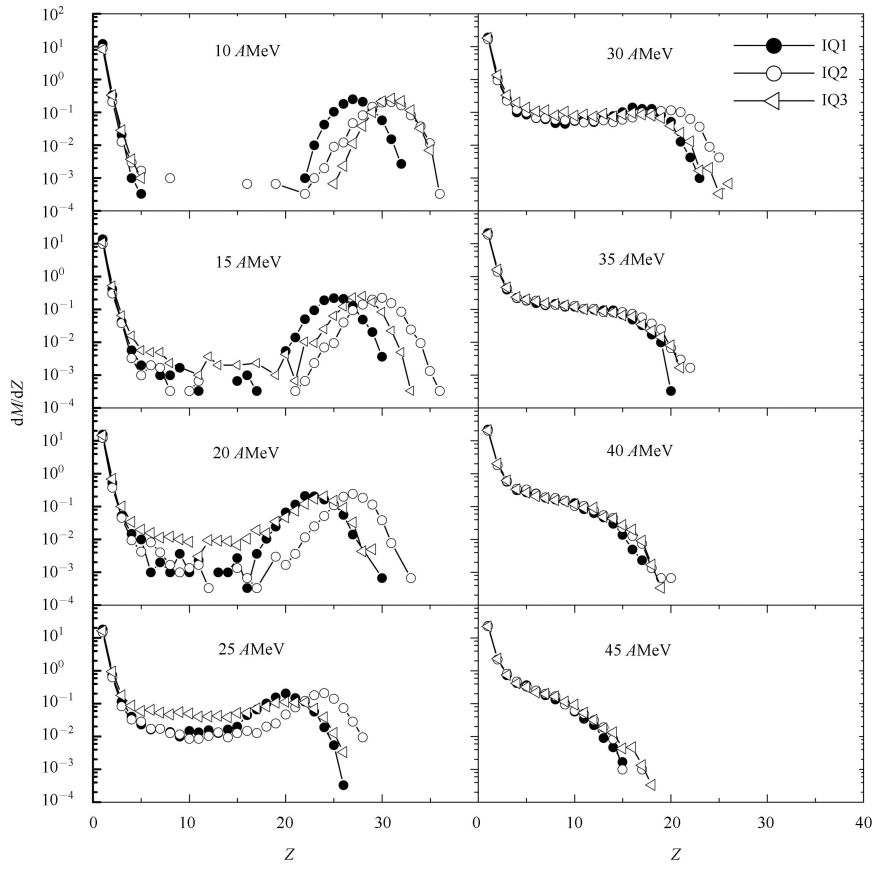
Fig. 4.   Charge distribution of fragments from three sets of parameters for ^{40}Ca+^{40}Ca at incident energies from 10 to 45 A MeV. The solid circles, open circles and open triangles denote the results with the IQ1, IQ2 and IQ3, respectively.
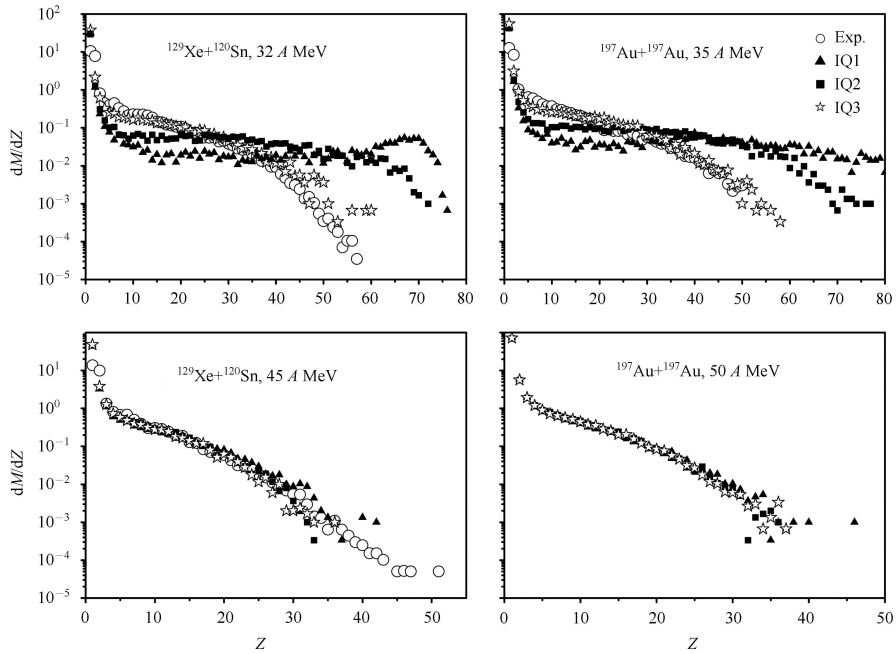

Fig. 5.   Charge distribution of fragments for ^{129}Xe+^{120}Sn at 32 and 45 A MeV, ^{197}Au+^{197}Au at 35 and 50 A MeV. The solid triangles, solid squares, open stars and open circles denote the results with the IQ1, IQ2, IQ3 and the experimental data, respectively. The ^{197}Au+^{197}Au at 50 A MeV does not give the experimental data.
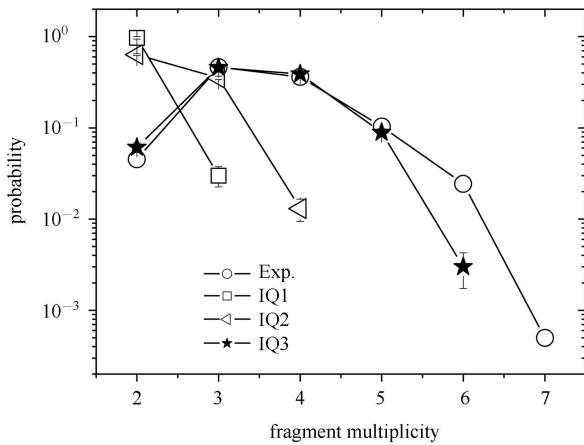
Fig. 6.   Fragment multiplicity spectrum of ^{238}U+^{197}Au reaction at 15 A MeV.

4   Summary

The N-N interaction has been investigated by using the ImQMD model with three sets of parameters IQ1, IQ2 and IQ3. The charge distribution of fragments at different incident energies were calculated based on the three sets of parameters. The calculation results demonstrate that the charge distribution and the fragment multiplicity spectrum are good observables for testing the model and the Fermi energy region is a sensitive energy region for probing the N-N interaction. The charge distribution of fragments below the threshold energy of nuclear multifragmentation are very sensitive to the ImQMD parameters. It is well known that the mean field significantly affects the whole nuclear reaction process in low energy heavy-ion collisions. The mean field for the three sets of parameters is different due to the different Skyrme type effective nucleon-nucleon interactions. With the increasing of incident energies, the two-body collisions and the non-equilibrium emission become more and more important, and the mean field effects on the charge distribution of fragments weakens gradually. The incompressibility coefficient for the IQ3 is 226 MeV which is in good agreement with the experimental data (230 ± 10 MeV), and the wave-packet width adopted in IQ3 is suitable for describing both the nuclear stability and central density of nuclei. By comparing the charge distribution of fragments and fragment multiplicity spectrum with the experimental data, we find that the IQ3 can not only be successfully applied for fusion reactions at low energy but also for heavy-ion collisions at the Fermi energy region.

References

1   WEI N, ZHOU X R, CHEN F Q. Chinese Physics C (HEP & NP), 2009, **33**: 116–118
2   Bertsch G F, Sabbey B et al. Phys. Rev. C, 2005, **71**: 054311
3   Brown B A, Richter W A, Lindsay R. Physics Letters Section B, 2000, **438**: 49–54
4   Dutra M, Delfino A et al. International Journal of Modern Physics D, 2010, **19**: 1583–1586
5   Klüpfel P, Reinhard P et al. Phys. Rev. C, 2009, **79**: 034310
6   CHEN L W, CAI B J, KO C M et al. Phys. Rev. C, 2009, **80**: 014322
7   Bartel J, Quentinet P et al. Nucl. Phys. A, 1982, **386**: 79–100
8   Dobaczewski J, Flocard H, Treiner J. Nucl. Phys. A, 1984, **422**: 103–139
9   Chabanat E, Bonche E, Haensel E et al. Nucl. Phys. A, 1998, **635**: 231–256
10   Waroquier M, Heyd K, Wenes G. Nucl. Phys. A, 1983, **404**: 269–297
11   SUN X Y, FANG D Q, MA Y G et al. Chinese Physics C (HEP & NP), 2011, **35**: 555–560
12   CHEN L W, KO C M, Li B A. International Journal of Modern Physics E, 2006, **15**: 1385–1395
13   Jain D, Kumar R, Sharma M K. Phys. Rev. C, 2012, **85**: 024615
14   WANG N, ZHAO K, Scheid K, WU X Z. Phys. Rev. C, 2008, **77**: 014603
15   FENG Z Q, JIN G M. Phys. Rev. C, 2009, **80**: 037601
16   Vautherin D, Brink D M. Phys. Rev. C, 1972, **5**: 626–647
17   Skyrme T H R. Philosophical Magazine, 1956, **1**: 1043–1054
18   Bell J S, Skyrme T H R. Philosophical Magazine, 1956, **1**: 1055–1068
19   Skyrme T H R. Nucl. Phys. A, 1959, **9**: 615–634
20   WANG N, LI Z X, WU X Z. Phys. Rev. C, 2002, **65**: 064608
21   WANG N, LI Z X, WU X Z, TIAN J L, ZHANG Y X, LIU M. Phys. Rev. C, 2004, **69**: 034608
22   WANG N, LI Z X, WU X Z et al. Mod. Phys. Lett. A, 2005, **20**: 2619–2628
23   ZHANG Y X, Danielewicz P et al. Phys. Lett. B, 2008, **664**: 145–148
24   Zanganeh V, WANG N, Ghodsi O N. Phys. Rev. C, 2012, **85**: 034601
25   ZHANG Y X, LI Z X. Phys. Rev. C, 2006, **74**: 014602
26   JIANG Y Y, WANG N, LI Z X, Scheid W. Phys. Rev. C, 2010, **81**: 044602
27   WANG N, WU X Z, LI Z X. Phys. Rev. C, 2003, **67**: 024604
28   Hagel K, Gonin M, Wada R et al. Phys. Rev. Lett, 1992, **68**: 2141–2144
29   Hudan S, Chbihi A, Frankland J D et al. Phys. Rev. C, 2003, **67**: 064613
30   D'Agostino M, Mastinu P F, Milazzo P M et al. Physics Letters B, 1996, **368**: 259–265
31   Vermani Y K, Chugh R, Sood A D. Ukrainian Journal of Physics, 2010, **55**: 1071–1077
32   D'Enterria D G, Fernández F, Luguera E et al. Phys. Rev. C, 1995, **52**: 3179–3188